Chapter 1

TOTAL INTERNAL REFLECTION FLUORESCENCE SPECTROSCOPY

Andrew J. de Mello

CONTENTS

0-8493-8352-8/96/$0.00+$.50

I. INTRODUCTION

The investigation and understanding of molecules at or in the vicinity of a surface is central to a variety of phenomena in the biological sciences. For example, the interaction of plasma proteins with foreign surfaces, the binding to and triggering of cells by hormones and neurotransmitters, photosynthetic reactions, antibody–antigen interactions, and cell attachment to surfaces are all interfacial processes and as such are distinct from bulk phase phenomena.[1-4]

Of particular interest is the adsorption of proteins and enzymes to material surfaces. It is known that when a foreign material contacts blood the initial response is adsorption of plasma proteins to form a secondary surface on top of the material. This surface is termed the "conditioning layer," and its structure and composition determine all subsequent blood–material interactions. This is of immense importance in the development of blood- and tissue-compatible materials, since it is recognized that the physiochemical nature of the conditioning layer influences the thrombogenic response of the blood to the biomaterial.[2]

Several techniques have been used to study the adsorption of biological molecules to solid surfaces. These include ellipsometry,[5] electrophoresis,[6] fluorescence spectroscopy,[7] infrared spectroscopy,[8] contact angle analysis,[9] Raman spectroscopy,[10] surface plasmon resonance,[11] and radiolabeling.[12] The suitability of any technique to the study of protein adsorption can be judged on the amount of information the technique can provide, i.e.

1. Is the technique quantitative?
2. Can conformational changes of the adsorbed species be monitored?
3. Can it provide dynamic information about adsorption and desorption processes?
4. Does the technique differentiate between bulk and surface-associated species?
5. Does the technique provide depth resolution (from surface to bulk)?
6. Is the technique applicable to all surfaces and all molecules?
7. Is the technique nondestructive and capable of *in situ* sensing?

An optical approach designed to satisfy the above criteria is Total Internal Reflection Fluorescence Spectroscopy (TIRFS). The technique is more correctly termed Evanescent Wave Induced Fluorescence Spectroscopy (EWIFS), but will be referred to as TIRFS in the current review. If used to its fullest extent, TIRFS can satisfy all the above parameters, and thus become a powerful surface analysis technique.

Much of the pioneering work in the field of internal reflection techniques was performed by Harrick in the 1960s.[13] Nevertheless, the first report of TIRFS was made by Hirschfield in 1965.[14] Since its inception, TIRFS has been used to investigate a diversity of species in the interfacial environment. These have ranged from proteins to polymers and dyes. The field of internal reflection fluorescence spectroscopy has been extensively reviewed in the literature. Critiques on TIR theory,[15] the application of TIRFS to protein adsorption studies,[16] TIRF quantitation methods,[17] time-resolved TIRFS,[18] multiple internal reflection fluorescence spectroscopy,[19] and the application of TIRFS to the investigation of polymer-surface interactions[20] are all available.

The applicability of TIRFS to a diversity of fields has meant that differing emphases have been put on contrasting aspects of the technique. The aim of this chapter is to introduce the fundamental ideas behind TIRFS and subsequently link together all the principal developments. It is designed to be an uncomplicated read that still contains the full concepts and essential ideas. The theory, experimental details, and potentials of TIRFS will be introduced to the reader in Chapter 1, while Chapter 2 will illustrate how TIRFS has been used to investigate a diversity of biological phenomena. The concepts presented in this chapter only assume that the reader possesses an understanding of elementary optics and photophysics.

II. A THEORETICAL DISCUSSION OF TOTAL INTERNAL REFLECTION

A. The Behavior of Light at a Dielectric Interface

When a plane wave, propagating through a transparent dielectric medium of high refractive index, encounters an interface with a similar medium of lower refractive index, one of two phenomena may occur. For near normal incidence, the incident beam will give rise to a plane, reflected beam in medium 1, together with a plane, transmitted beam in medium 2 (Figure 1.1a). The reflected wave propagates at an angle equal and opposite to that made by the incident wave, and the properties of the transmitted wave are defined according to Snell's Law, i.e.

$$n_1 \sin\theta_i = n_2 \sin\theta_t \qquad \textbf{(1.1)}$$

where n_1 and n_2 refer to the refractive indices of each medium. Since $n_1 > n_2$,

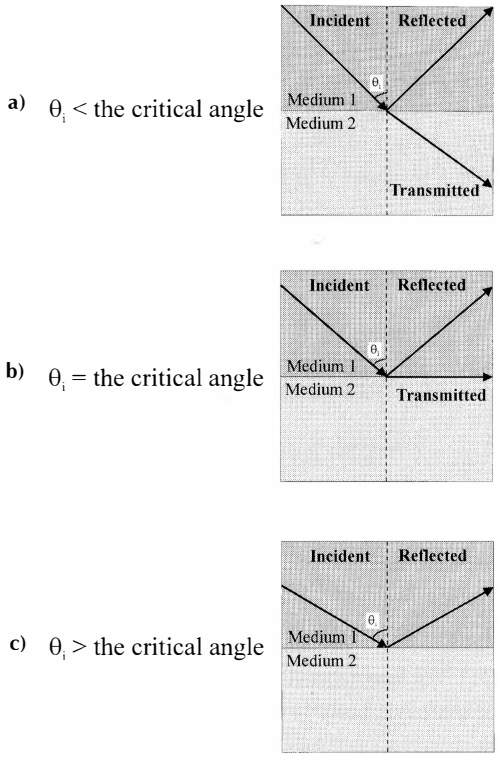

Figure 1.1
(a) Electromagnetic radiation incident on the interface between two media, where $n_1 > n_2$, and $\theta_i < \theta_c$. (b) Electromagnetic radiation incident on the interface between two media, where $n_1 > n_2$, and $\theta_i = \theta_c$. (c) Electromagnetic radiation incident on the interface between two media, where $n_1 > n_2$, and $\theta_i > \theta_c$.

$$\frac{n_1}{n_2} = \frac{\sin\theta_t}{\sin\theta_i} > 1 \qquad \textbf{(1.2)}$$

Therefore, $\theta_t > \theta_i$, and the transmitted wave in medium 2 is always 'bent' away from the normal. This change in direction must occur at the interface to account for the phase continuity of the electromagnetic field across the interface plane, and the fact that electromagnetic waves travel faster in the less dense medium.

If θ_i is increased until it reaches $\sin^{-1}(n_2/n_1)$, the angle θ_t becomes 90° ($\pi/2$ radians). In this situation, the transmitted wave travels parallel to the interface, as illustrated in Figure 1.1b. The angle of incidence generating these conditions is termed the critical angle. It is noted that if the plane wave were to be incident in the less dense medium θ_t could never reach 90°, thus forbidding the existence of a critical angle.

If the angle of incidence exceeds this critical angle there is no real solution to Snell's Law, since n_2/n_1 cannot exceed 1. Therefore, the existence of a propagating, transmitted wave in the lower refractive index medium is forbidden, and all the incident energy is reflected back into medium 1. This phenomenon is commonly termed Total Internal Reflection (TIR), and is illustrated in Figure 1.1c.

The angular behavior of electromagnetic radiation at an interface can be more completely described through the use of Fresnel's equations.[20] These equations simply define the reflected and transmitted electric field amplitudes for unit incident electric field amplitudes. If we consider incident radiation polarized with the electric field vector perpendicular to the plane of incidence,* an amplitude reflection coefficient can be defined as,

$$r_\perp = \left\{\frac{E_{0r}}{E_{0i}}\right\} = \frac{n_1\cos\theta_i - n_2\cos\theta_t}{n_1\cos\theta_i + n_2\cos\theta_t} \qquad \textbf{(1.3)}$$

where E_{0r} and E_{0i} are the reflected and incident beam electric field amplitudes. (The derivation of these equations is unnecessary for the current discussion.) The amplitude transmission coefficient can be similarly defined as,

$$t_\perp = \left\{\frac{E_{0t}}{E_{0i}}\right\} = \frac{2n_1\cos\theta_i}{n_1\cos\theta_i + n_2\cos\theta_t} \qquad \textbf{(1.4)}$$

These expressions are intuitively appealing. For example, if two adjacent media have the same refractive index, the amplitude reflection coefficient is zero, and the amplitude transmission coefficient is unity. However, it is noted that the amplitude reflection coefficient is finite at normal incidence when $n_2 \neq n_1$ (e.g., normal incidence for a fused-silica/air interface ($n_1 = 1.467$ and $n_2 = 1$) yields $r_\perp$ equal to 0.189).

From Fresnel's Equations (which describe electric field amplitudes), expressions for the interfacial reflectance and transmittance can be developed. The reflectance, R, is defined as the ratio of the reflected power to the incident power, and can be mathematically described as,

$$R = \left\{\frac{E_{0r}}{E_{0i}}\right\}^2 = r_\perp^2 \qquad \textbf{(1.5)}$$

* For simplicity, only perpendicular polarized electromagnetic fields are considered. Corresponding equations for parallel polarization are more complicated, but yield quantitatively similar results.

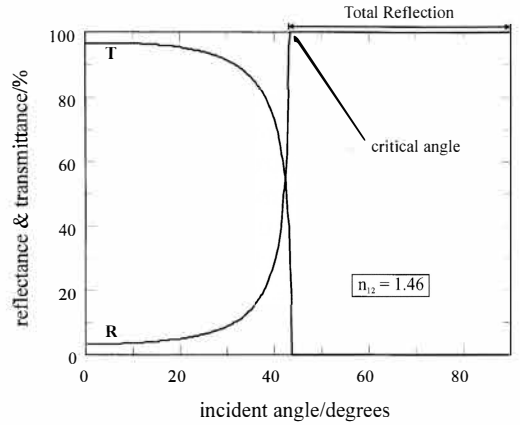

Figure 1.2
Reflectance as a function of incident angle for an interface between media with refractive indices $n_1 = 1.46$ and $n_2 = 1$. Incident electromagnetic radiation is polarized perpendicular to the plane of incidence. $\theta_c = 43.23$ degrees.

Similarly, the transmittance, T, represents the ratio of the transmitted power to the incident power, i.e.,

$$T = \left(\frac{n_2 \cos\theta_t}{n_1 \cos\theta_i}\right)\left\{\frac{E_{0r}}{E_{0i}}\right\}^2 = \left(\frac{n_2 \cos\theta_t}{n_1 \cos\theta_i}\right) t_\perp^2 \qquad \textbf{(1.6)}$$

Here, T does not simply equal $t_\perp^2$. The ratio n_2/n_1 is present to account for the difference in the rate at which energy is transported into and out of the interface, and the ratio of the cosine terms demonstrates that the cross-sectional areas of the incident and transmitted beams are different.

Figure 1.2 illustrates the variation of both R and T with angle of incidence for a fused-silica/air interface. For perpendicular polarization, the reflectance equals 3.58% at normal incidence. As θ_i increases, the reflectance grows until it reaches 100% at the critical angle. For angles greater than the critical angle, the transmitted angle turns imaginary since $\sin^2\theta_i > (n_{21})^2$, where $n_{21} = n_2/n_1$. Thus, R = 100%. Now the transmitted angle may be obtained from

$$\cos\theta_t = \left(1 - \sin^2\theta_t\right)^{1/2} = i\frac{\left(\sin^2\theta_i - \left(n_{21}\right)^2\right)^{1/2}}{\left(n_{21}\right)} \qquad \textbf{(1.7)}$$

Conversely, T equals 96.42% for normal incidence and diminishes until it reaches 0 at the critical angle. It is noted that the sum of T and R for a

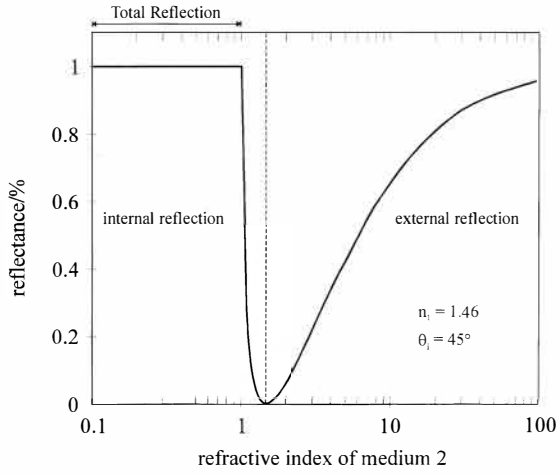

Figure 1.3
Reflectance as a function of the refractive index of medium 2. $\theta_i = 45$ degrees and $n_1 = 1.46$. The dotted, vertical line represents the division between the internal and external reflection regimes.

given angle of incidence is always 100%. This fact is in agreement with the Law of Conservation of Energy and demonstrates that energy is maintained across the interface.

The magnitude of R and T is also dependent on the ratio of n_2 to n_1. Figure 1.3 describes the variation of R with the refractive index of the medium 2. If n_1 and the angle of incidence are fixed, it can be seen that R describes a complicated function. When n_2 is less than a critical index (given by $n_1 \sin\theta_c$), R remains constant and equal to 100%. As n_2 increases, R drops sharply and reaches zero when $n_2 = n_1$. Any further increase in n_2 will cause a corresponding increase in R. Hence, Figure 1.3 can be separated into two zones: Zone 1 describing internal reflection ($n_{21} < 1$), and Zone 2 describing external reflection ($n_{21} > 1$). It is important to observe that internal reflection is far more sensitive to changes in the refractive index of medium 2, than external reflection.

B. Existence of a Boundary Wave

Section II.A described the behavior of electromagnetic radiation at an interface between two transparent, homogeneous, dielectric media. It appeared that within the regime of total internal reflection all incident radiation remained in the high refractive index medium, and no energy was transmitted across the interface. However, if the lower refractive index medium is modified so that it is able to absorb electromagnetic radiation of the same characteristics as the incident radiation, the situation becomes far more involved.

For two nonabsorbing media it is realized that TIR occurs when $n_1 > n_2$ and $\theta_i > \theta_c$. Under these conditions the intensity (the energy per unit area per unit time) of the incident wave (I_{inc}) is identical to the intensity of the reflected wave (I_{refl}).

$$I_{inc} = I_{refl} \tag{1.8}$$

Therefore, the interfacial reflectance, R is 100%, i.e.

$$R_{non-abs} = \frac{I_{refl}}{I_{inc}} = 1 \tag{1.9}$$

Now, if medium 2 is modified so that it is able to absorb radiation of similar characteristics to the incident radiation, the following inequality can be written:

$$R_{abs} = \frac{I_{refl}}{I_{inc}} < 1 \tag{1.10}$$

This trivial statement demonstrates that the intensity of the reflected beam is less than the intensity of the incident beam. Since only the characteristics of medium 2 have been altered, this must imply that the incident radiation has crossed the interface, interacted with the absorbing medium, and then returned back into medium 1. This situation is termed Attenuated Total Reflection (ATR). Now, the fractional reduction in the interfacial reflectance is equal to the fraction of incident radiation absorbed (Δ) and can be expressed as

$$\Delta = \frac{(I_{inc} - I_{refl})}{I_{inc}} = 1 - \left(\frac{I_{refl}}{I_{inc}}\right) = 1 - R_{abs} \tag{1.11}$$

The manner in which the incident wave crosses the interface into medium 2, and then returns back into medium 1, had been a subject of much controversy since it was first observed by Sir Isaac Newton in the 17th century.[21] The advent of Maxwell's equations in the mid 19th century provided the means to understand this phenomenon.[22] The equations predicted the existence of an electromagnetic disturbance in medium 2. The properties of this disturbance are discussed in the following section. The mathematical derivation is only stated for completeness. Nevertheless, the physical concepts generated from the mathematics are important in understanding the nature of the interfacial field.

C. Characteristics of the Boundary Wave

To derive the properties of the boundary wave, the general interfacial system outlined in Figure 1.1a is examined in detail. If the incident wave in medium 1 is considered to be planar and monochromatic (for simplicity), it can be described, according to Maxwell's equations, by the following expression:

$$E_I = E_{0i} \exp\left[i(\omega_i t - k_i \cdot r)\right] \tag{1.12}$$

Here E_I represents the electric field amplitude at a point r at time t (E_{0i} is constant in time). The vector k points in the direction of propagation and its magnitude is the wavenumber (= ω/c). The quantity ω is the oscillation frequency of the wave, and c is the velocity of the wave in medium 1. Furthermore, for a transparent, dielectric medium of refractive index n,

$$\omega^2 = \frac{c_0^2 \cdot k^2}{n^2} \tag{1.13}$$

where, c_0 is equal to the velocity of light *in vacuo*. If the incident wave propagating through medium 1 impinges on the boundary with medium 2, a reflected and transmitted wave can be produced (this is the only assumption made). A coordinate system is chosen so that the boundary is the yz plane and perpendicular to the incident wave surfaces. Hence, the propagation vectors of the incident, reflected, and transmitted waves can be described according to Figure 1.4.

The following solutions to the electromagnetic wave equations can be stated,

$$E_R = E_{0r} \exp\left[i(\omega_r t - k_r \cdot r)\right] \quad \text{for the reflected wave} \tag{1.14}$$

$$E_T = E_{0t} \exp\left[i(\omega_t t - k_t \cdot r)\right] \quad \text{for the transmitted wave} \tag{1.15}$$

In the vicinity of the boundary, the electric fields of the incident and reflected waves superpose, causing a standing electromagnetic wave to be established in medium 1. Thus, the total electric field in each medium may be given by

$$E_{med.1} = E_I + E_R \tag{1.16}$$

$$E_{med.2} = E_T \tag{1.17}$$

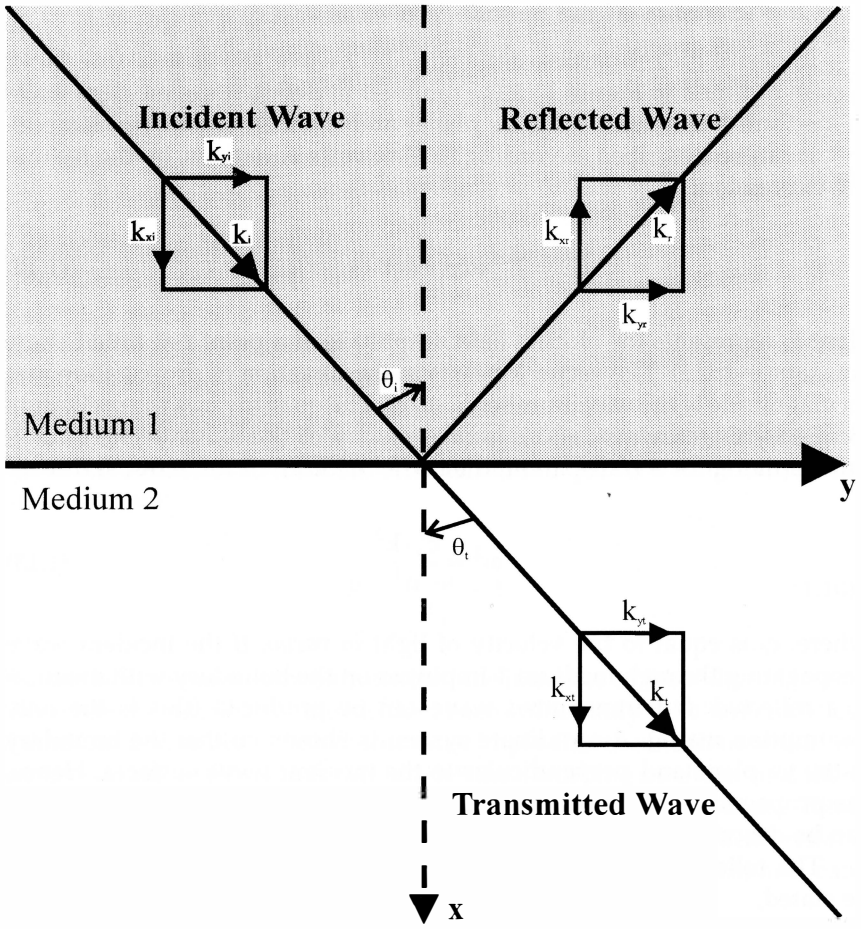

Figure 1.4
Electromagnetic radiation incident at an angle θ_i in the yx plane to an interface in the yz plane, separating two dielectric media of refractive indices n_1 and n_2. The propagation vectors of the incident, reflected and transmitted electric fields are given by k_i, k_r, and k_t, respectively.

Furthermore, at the boundary

$$E_T = E_I + E_R \qquad \textbf{(1.18)}$$

If Equation 1.18 is combined with Equations 1.12–1.15 when $\theta_i \geq \sin^{-1} n_{21}$ (TIR conditions), a general expression for the transmitted electric field amplitude can be generated, i.e.,

$$E_T = E_{0t} \exp \pm \left(\left(\frac{\omega^2}{c^2} \right)^{1/2} \left[n_2^2 - n_1^2 \sin^2 \theta_i \right]^{1/2} .x \right) . \exp i\left(\omega t - k_{yI} .y\right) \qquad \textbf{(1.19)}$$

This complex equation describes the transmitted wave when the angle of incidence is greater than the critical angle. It simply states that the electric field amplitude of the transmitted wave either grows or decays exponentially with distance away from the boundary (into medium 2). It is physically untenable to expect E_T to expand exponentially with distance away from the interface. If this were the case, an electric field of exceptionally high magnitude would occur within only a few wavelengths of the boundary. Clearly, E_T must decay exponentially with increasing distance into medium 2. Hence, under the conditions of TIR the transmitted electromagnetic field is termed an evanescent wave, and has the form:

$$E_T = E_{0t} \exp - \left(\left(\frac{\omega^2}{c^2} \right)^{1/2} \left[n_2^2 - n_1^2 \sin^2 \theta_i \right]^{1/2} .x \right) . \exp i\left(\omega t - k_{yI} .y\right) \qquad \textbf{(1.20)}$$

The evanescent wave is an inhomogeneous, electromagnetic wave, where the planes of constant phase and constant amplitude do not coincide.[18] It is noted that the mathematical description of the transmitted field is separated into two parts. The first exponential term accounts for the evanescent decay of the transmitted wave into medium 2 (i.e., in the x-direction), whereas the second exponential term describes a propagating electromagnetic component in the y-direction. This demonstrates that the surface wave concurrently propagates along the interface and decays perpendicularly to it.

The existence of the propagating term (in Equation 1.20) is evidenced by the fact that a total internally reflected wave is displaced upon reflection from an interface. This displacement is termed the Goos-Hänchen shift, and is illustrated in Figure 1.5. The magnitude of the shift is a fraction of a wavelength and is dependent on the angle of incidence and the polarization of the incident wave.[23]

For clarity, it is advantageous to simplify Equation 1.20 to

$$E(x) = E_0 \exp - \left(\frac{x}{d_p} \right) \qquad \textbf{(1.21)}$$

Here, E(x) is the electric field amplitude of the evanescent wave at a distance x from the interface, E_0 is the transmitted interfacial electric field amplitude per unit incoming amplitude, and d_p is termed the depth of

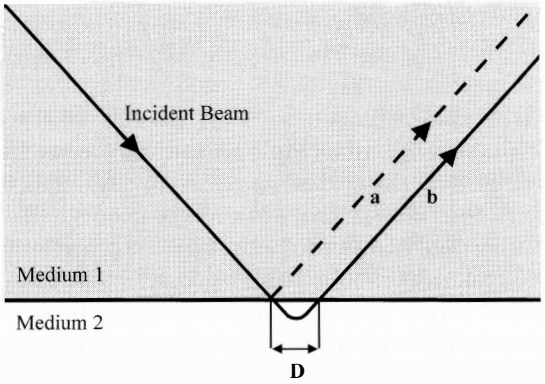

Figure 1.5
Schematic representation of the Goos and Hänchen displacement. Part (a) illustrates the path of the reflected beam when medium 2 is a perfect conductor (i.e., E = 0 at the interface). Part (b) illustrates the path of the reflected beam if medium 2 is a dielectric (i.e., E ≠ 0 at the interface).

penetration. This is an arbitrary quantity and defines the distance into medium 2, where the electric field amplitude has decreased to e^{-1} of its interfacial value. It can be mathematically approximated by

$$d_p = \left(\frac{\lambda_{vac}}{2.\pi.n_1}\right)\sqrt{\left(\frac{1}{\sin^2\theta_i - (n_{21})^2}\right)} \qquad \textbf{(1.22)}$$

where λ_{vac} is the wavelength of the incident radiation *in vacuo*. It is recognized that the magnitude of d_p is dependent on λ_{vac}, θ_i, n_1, and n_2. This effect will be used to good effect later.

Figure 1.6 describes the electric fields in both media under TIR conditions. It is observed that the superposition of incident and reflected waves establishes a standing-wave pattern in medium 1. The properties of the standing wave are dependent on the nature of both media. In the case of metallic reflection, medium 2 (the metal) is a perfect conductor. Hence, interfacial boundary conditions will constrain the electric field perpendicular to the interface to be zero at the interface. For this condition to be obeyed, the standing-wave is such that a node must exist in the interfacial plane. Conversely, when both media are dielectrics (as is the case here), boundary conditions forbid a discontinuity in the electric field at the interface. Thus, it is required that the transmitted, electric field amplitude at the interface be equal to the nonzero amplitude of the standing-wave at the interface. Physically, it is this nonzero electric field at the interface that allows the energy to move into medium 2 and form the characteristic evanescent wave.

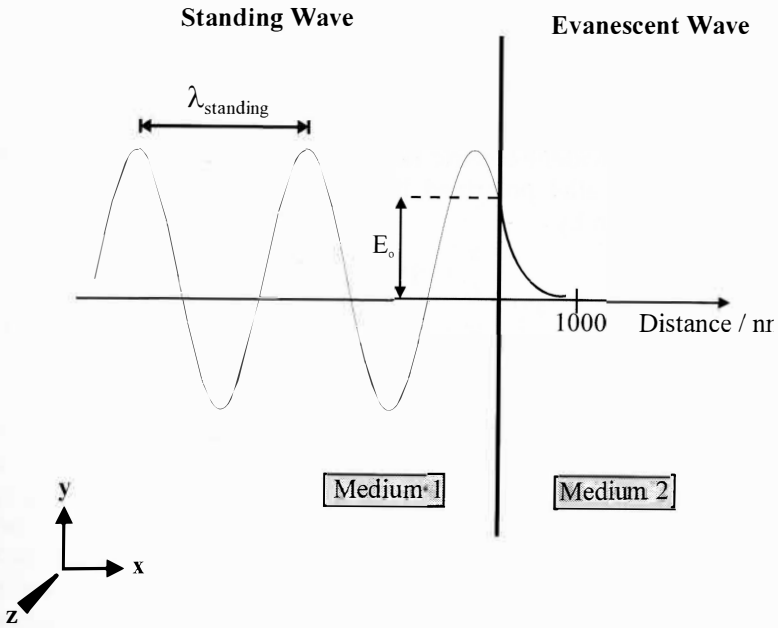

Figure 1.6
Standing wave pattern established in the vicinity of a totally reflecting interface. The electric field amplitude has a sinusoidal dependence on distance from the interface in medium 1, and an exponentially decaying amplitude with distance from the interface in medium 2. It is noted that E ≠ 0 at the interface.

For unpolarized light, the values of E_0 (the electric field amplitudes at the interface, but in medium 1) for the directions x, y, and z (defined in Figure 1.6) are given by

$$E_{0x} = \frac{2\sin\theta_i\cos\theta_i}{\left(1-n_{21}^2\right)^{1/2}\left[\left(1-n_{21}^2\right)\sin^2\theta_i - n_{21}^2\right]^{1/2}} \qquad \textbf{(1.23)}$$

$$E_{0y} = \frac{2\left(\sin^2\theta_i - n_{21}^2\right)^{1/2}\cos\theta_i}{\left(1-n_{21}^2\right)^{1/2}\left[\left(1-n_{21}^2\right)\sin^2\theta_i - n_{21}^2\right]^{1/2}} \qquad \textbf{(1.24)}$$

$$E_{0z} = \frac{2\cos\theta_i}{\sqrt{\left(1-(n_{21})^2\right)}} \qquad \textbf{(1.25)}$$

Therefore, if the incident electric field vector is perpendicular to the plane of incidence, the total electric field amplitude $E_\perp$, may be expressed as

$$E_{\perp} = E_{0z} = \frac{2\cos\theta_i}{\sqrt{\left(1-\left(n_{21}\right)^2\right)}} \tag{1.26}$$

However, if the incident electric field vector is parallel to the plane of incidence, i.e., parallel polarized light, then E_{ll} (the total electric field amplitude) is given by

$$E_{ll} = \left(\left|E_{0x}\right|^2 + \left|E_{0y}\right|^2\right)^{1/2} = \frac{2\cos\theta_i\left(2\sin^2\theta_i - n_{21}^2\right)^{1/2}}{\left(1-n_{21}^2\right)^{1/2}\left[\left(1-n_{21}^2\right)\sin^2\theta_i - n_{21}^2\right]^{1/2}} \tag{1.27}$$

This description is important since it illustrates that electric fields in all 3 spatial directions are present at the interface (the mathematics are only shown for completeness). This is in contrast to a conventional, propagating electromagnetic wave, where Maxwell's equations only allow electric fields to exist normal to the direction of propagation.[13] Consequently, the evanescent wave is unique among electromagnetic waves in possessing longitudinal character. Furthermore, the complex electric field structure permits dipoles of *any* orientation to absorb evanescent wave energy, whereas normal electromagnetic radiation can only be absorbed by dipoles which are not aligned parallel to the direction of propagation.

From an experimental point of view, it is far more useful to consider intensities of the electromagnetic field. Since $I \propto |\mathbf{E}|^2$, a new set of equations can be easily generated from Equations 1.23–1.27 to describe intensities at the interface (in medium 1), i.e.,

$$I_{0x} = \frac{4\sin\theta_i^2\cos\theta_i^2}{\left(1-n_{21}^2\right)\left[\left(1-n_{21}^2\right)\sin^2\theta_i - n_{21}^2\right]} \tag{1.28}$$

$$I_{0y} = \frac{4\left(\sin^2\theta_i - n_{21}^2\right)\cos^2\theta_i}{\left(1-n_{21}^2\right)\left[\left(1-n_{21}^2\right)\sin^2\theta_i - n_{21}^2\right]} \tag{1.29}$$

$$I_{0z} = \frac{4\cos^2\theta_i}{\left(1-\left(n_{21}\right)^2\right)} \tag{1.30}$$

and

$$I_{\perp} = I_{0z} = \frac{4\cos^2\theta_i}{\left(1-\left(n_{21}\right)^2\right)} \tag{1.31}$$

$$I_{ll} = I_{0x} + I_{0y} = \frac{4\cos^2\theta_i\left(2\sin^2\theta_i - n_{21}^2\right)}{\left(1-n_{21}^2\right)\left[\left(1-n_{21}^2\right)\sin^2\theta_i - n_{21}^2\right]} \tag{1.32}$$

Therefore, the intensity profile of the evanescent wave can be defined according to

$$I(x) = I_0 \exp -\left(\frac{x}{\Lambda}\right) \tag{1.33}$$

$$\Lambda = \frac{d_p}{2} = \left(\frac{\lambda_{vac}}{4.\pi.n_1}\right)\sqrt{\left(\frac{1}{\sin^2\theta_i - \left(n_{21}\right)^2}\right)} \tag{1.34}$$

Here, I(x) is the intensity of the evanescent wave at a distance x from the interface, I_0 is the interfacial intensity (at x = 0). Λ defines the distance at which the intensity of the evanescent wave has diminished to e^{-1} of its interfacial value. The magnitude of Λ is clearly dependent on a number of factors. Figure 1.7a–c graphically describes the intricate relationship between Λ and λ_{vac} / θ_i, / n_{21}. It is observed that changes in any of the experimental parameters will cause significant changes in the spatial characteristics of the evanescent wave. This can be used to good effect by the experimenter.

Finally, from Equation 1.34 it can be seen that there are 2 limiting values for Λ. In the lower limit $\theta_i = 90°$ ($\pi/2$ radians), and Λ becomes

$$\Lambda_{90°} = \frac{\lambda_{vac}}{4\pi n_1\sqrt{1-n_{21}^2}} \tag{1.35}$$

Conversely, as θ_i tends to θ_c, Λ tends to ∞ and refraction occurs, i.e., the transmitted electric field becomes a propagating wave. The variation in θ_i allows the experimenter to vary the depth that the evanescent wave penetrates into medium 2.

In summary, the transmitted wave generated under TIR conditions is closely associated with the surface. It is a surface specific, electromagnetic disturbance that advances in the y-direction as a surface wave, and exponentially decays (in the x-direction) as it penetrates into the less dense medium. Its properties are dependent on the characteristics of the incident light, the angle of incidence, and the refractive indices of both media.

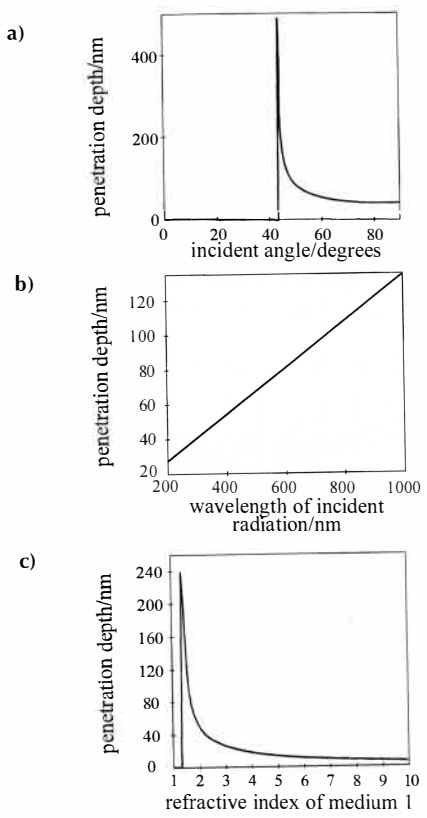

Figure 1.7
(a) Penetration depth of the evanescent wave as a function of incident angle for a glass/water interface: λ = 488 nm and n_{21} = 0.685. The penetration depth at the critical angle is infinitely large. (b) Penetration depth of the evanescent wave as a function of incident radiation wavelength for a glass/water interface: θ_i = 45 degrees and n_{21} = 0.685. (c) Penetration depth of the evanescent wave as a function of incident radiation wavelength for a glass/water interface: θ_i = 45 degrees and λ = 488 nm.

III. THE EVANESCENT WAVE AS A SPECTROSCOPIC TOOL

A. Absorption of the Evanescent Wave

The characteristics of the evanescent wave outlined in Section II.B are of particular interest to the spectroscopist. If the lower refractive index medium contains molecules which are able to absorb light, then a proportion of the evanescent energy can be removed before the radiation returns back into the high refractive index medium. This absorption is evidenced by a drop in the interfacial reflectivity. In ATR spectroscopy, the experimenter directly calculates the fraction of the incident wave

intensity that has been absorbed within the evanescent volume (i.e., Δ in Equation 1.11).[13,15] Measurement of Δ provides important structural and physical information in a manner akin to conventional absorption and transmission spectroscopy.

For a bulk solution, the intensity of a beam entering an absorbing sample (I_{in}) will diminish exponentially at a rate defined by the product of the bulk solute concentration (c), the molar naperian absorption coefficient (α), and the distance traversed through the sample (x). Hence, the absorption, A, can be defined as

$$A = \frac{I_{in} - I_{out}}{I_{in}} = \frac{k.c}{I_{in}} \int_0^l I_{in} \exp(-\alpha.c.x)\,dx \qquad \textbf{(1.36)}$$

where l is the beam path length, I_{out} is the beam intensity emerging from the sample, and k is an arbitrary constant. When l is ∞, A=1 and $k = \alpha$, thus

$$A = \frac{\alpha.c}{I_{in}} \int_0^l I(x)\,dx \qquad \textbf{(1.37)}$$

In an analogous fashion, an expression for the fractional absorption of evanescent intensity, by chromophores near the interface, can be developed. Combination of Equations 1.11 and 1.36 yields

$$\Delta = \frac{(I_{inc} - I_{refl})}{I_{inc}} = \frac{\alpha}{I_{inc}} \int_0^\infty c(x)I(x)\,dx \qquad \textbf{(1.38)}$$

and since I(x) is defined according to Equation 1.33, the expression for evanescent absorption is given by

$$\Delta = a.c.\left(\frac{I_0}{I_{inc}}\right).\Lambda = \alpha.c.d_e \qquad \textbf{(1.39)}$$

Here d_e is defined as the 'effective thickness' and equal to $(I_0 / I_{inc})\Lambda$. The physical significance of this parameter has been addressed by both Harrick and Reichert.[13,15] In broad terms, d_e is analogous to the beam pathlength in conventional absorption techniques, and thus is a measure of the interaction of the evanescent wave with the absorbing sample. This is quite distinct from the penetration depth of the evanescent wave, which describes how far the electromagnetic disturbance travels into the less dense medium. The penetration depth is polarization independent, whereas the effective thickness is polarization dependent.

In essence, if medium 2 is a solution (e.g., protein in buffer), then molecules in the proximity of the interface (within a few hundred nm)

are able to absorb evanescent radiation of particular wavelengths. The wavelengths that are absorbed and the efficiency of the absorption depend on both the structure and the environment of the molecule. Thus, ATR is a useful tool for characterizing how molecules behave in the vicinity of an interface.

B. Evanescent Wave Induced Fluorescence

Fluorescence spectroscopy is an alternative to absorption spectroscopy. Absorption processes involve promotion of a molecule from a ground state electronic energy level to an excited state energy level. Once in the excited state, the molecule can lose the excess energy in a variety of ways. If deactivation of the excited state occurs through emission of electromagnetic radiation, then the process is termed luminescence, and in particular fluorescence. The parameters of fluorescence are extremely sensitive to environmental changes, and typically fluorescence can be detected at chromophore concentrations that are 2 to 3 orders of magnitude below those used for absorption measurements. Furthermore, since there are many processes that occur on the same time scale as the excited state decaytime (10^{-12} to 10^{-6} s), fluorescence is routinely used to probe molecular structure and conformation, molecular motion, energy transfer processes, and solvent rearrangements.[24,25] In contrast, absorption of electromagnetic radiation occurs in ~10^{-15} s. During this period the state of the chromophore and its environment will remain essentially static.

Accordingly, the surface-specific evanescent wave can be used to excite fluorescence from molecules in the vicinity of the interface. This is the basis of TIRFS or EWIFS (evanescent wave induced fluorescence spectroscopy). In a similar manner to ATR, the evanescent wave energy is absorbed by a molecule. However, now the experimenter investigates the characteristics of the re-emitted radiation, rather than the attenuation of the incident beam.

The evanescent wave induced fluorescence measured does not directly correlate with the amount of energy absorbed by the sample. As stated previously, a molecule promoted into an excited state through absorption of energy can lose its energy in a variety of ways. Broadly speaking, deactivation occurs via radiative or nonradiative pathways. The nonradiative pathways compete with fluorescence to depopulate the excited state. This causes a faster decay of the excited state population than would be expected if fluorescence was the sole deactivation channel. Consequently, the observed fluorescence decaytime is less than the radiative lifetime. To quantify this deviation, the term *fluorescence quantum efficiency* is introduced. The fluorescence quantum efficiency, ϕ_f, defines the fraction of excited state species that become de-excited by fluorescence, and is given by

$$\phi_f = \frac{k_r}{k_r + k_{nr}} \tag{1.40}$$

where k_r = radiative deactivation rate constant and k_{nr} = nonradiative deactivation rate constant. Since TIRFS measures the amount of absorbed, evanescent energy that is re-emitted as fluorescence, the following expression is valid.

$$I_f = \Delta \phi_f \tag{1.41}$$

where I_f is the evanescent wave induced fluorescence intensity. I_f is more completely described by Equation 1.42.[26]

$$I_f \propto \int_0^\infty \phi_f . c(x) . I_0 \exp(-x/\Lambda)\, dx \tag{1.42}$$

This expression describes I_f for a fluorophore in solution. It simply states that if the fluorescence quantum efficiency of the fluorophore is constant, evanescent wave induced fluorescence intensities directly relate to surface concentrations, making TIRFS a quantitative tool. Furthermore, any variations in the spectral or temporal characteristics of the fluorescence emission can provide valuable information about the immediate environment and conformation of the fluorophore. Most biomolecules fluoresce intrinsically due to the existence of the aromatic amino acid residues tryptophan, tyrosine, and to a lesser extent phenylalanine.[16] These residues absorb in UV region of the electromagnetic spectrum, and their emission is extremely sensitive to the local environment (e.g., pH and solvent). Consequently, structural changes in the biomolecule can often be inferred from variations in the observed photophysics. It is further noted that most proteins will contain more than one fluorescent residue (e.g., bovine serum albumin contains two tryptophan residues in different environments). This greatly complicates the characteristics of the observed emission. The analysis of intrinsic fluorescence is thus governed by empirical rules obtained from studies on "model" compounds whose structural characteristics are well defined. However, nature is not always kind, and many important biomolecules are bereft of fluorescent groups. To overcome this problem, an extrinsic fluorophore (most commonly a small, rigid dye molecule) is introduced into the biomolecule, either through simple binding or via chemical coupling.[17] Thus, the behavior of the parent molecule can be monitored through variations in the photophysics of the label. The extrinsic fluorophore must be tightly bound at a unique location, have photophysical properties dependent on environment, and most important, it must not affect the physical characteristics of the parent molecule.

Common extrinsic fluorophores include acridine orange, fluorescein, rhodamine B, and ethidium bromide. The use of extrinsic fluorescence is appealing since it typically involves fluorophores that absorb in the visible region of the spectrum. Also, if different labels are used, the possibility of competitive adsorption studies is provided for (i.e., analysis of systems containing more than one adsorbing species).

To address the practicalities and subtleties of the technique, it is advantageous to separate the discussion into two parts. At the first level, steady-state TIRFS provides a means of monitoring molecular adsorption and desorption, semi-quantifying surface concentrations, and investigating surface-induced conformational changes. Secondly, time-resolved TIRFS extends the technique into the time domain and allows the methodology to be made fully quantitative. The use, instrumentation, and applications of the two variations are accordingly discussed in Sections IV and V.

IV. STEADY-STATE TIRF SPECTROSCOPY

A. Instrumentation

A generic experimental set-up for steady-state TIRF spectroscopy is schematically illustrated in Figure 1.8. For clarity, the apparatus can be envisaged as consisting of 3 sections: the light source, the EWIF sample stage, and the fluorescence detection/analysis system.

The Light Source. The fundamental part of many spectroscopic techniques is a laser. As light sources, lasers possess distinct qualities that make them superior to most conventional lamp systems. Laser excitation generates coherent, collimated radiation of appreciable intensity, which can be pulsed at very high repetition rates (≤100MHz). Through use of pumped dye laser systems, a wide range of lasing wavelengths can be obtained (200 to 1300nm), thus allowing a diversity of species to be studied. As noted previously, promotion of a molecule from its ground state to an excited electronic state is a prerequisite for fluorescence. IR radiation is not sufficiently energetic to excite the required transitions, thus confining TIRFS to the UV and visible regions of the electromagnetic spectrum. In any TIRFS experiment, choice of the exciting wavelength is dependent on the absorption profile of the fluorophore in medium 2. Laser excitation is of particular use in TIRFS, since the incident beam can be focused tightly on the interfacial plane. This ensures the production of a well-defined EWIF spot, which can be imaged effectively.

The EWIF Sample Stage. The heart of the experimental set-up is the EWIF sample stage. This consists of an internal reflection element (IRE) in contact with the sample under study. The additional use of a disposable surface between the IRE and sample allows the characteristics of the

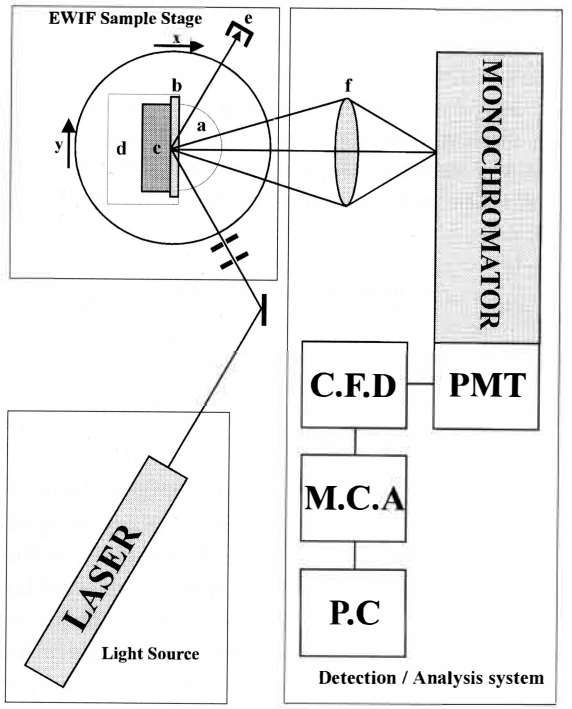

Figure 1.8
Schematic of steady-state TIRF spectrometer: (a) Hemicylindrical prism, (b) Quartz surface, (c) Flow cell containing sample, (d) Rotation stage mounted on an xy translation stage, (e) Beam stop, (f) High numerical aperture collection lens. (PMT - Photomultiplier Tube, CFD - Constant Fraction Discriminator, MCA - multichannel analyzer, PC - personal computer).

surface to be varied. The purpose of the IRE is to guide the incident beam to the interface at a desired angle and to generate TIR conditions. Subsequently, the evanescent wave produced in medium 2 excites fluorescence from within the sample. Visually, this is observed as a fluorescence spot. The IRE must be transparent in the UV-visible region of the spectrum, nonfluorescent, and possess highly polished surfaces. Any significant roughness in the reflecting surface will lead to extraneous and unwanted scatter. Scatter-induced fluorescence is a significant problem in TIRFS and will be discussed in detail in Section IV.3.[17] A diversity of TIR prisms is available, however the hemicylindrical design shown in Figure 1.8 is advantageous since the incident and reflected beams travel normally through the curved surface. This minimizes multireflections and scatter. The design is also suited to the measurement of angular TIRF spectra. As previously remarked, the penetration depth of the evanescent wave is dependent on θ_i. As θ_i increases, the penetration depth of the evanescent wave decreases (i.e., the evanescent wave becomes more closely associated with the surface). Accordingly, the evanescent wave induced

fluorescence will contain more information about surface associated species relative to bulk solution species as the incident angle is increased. To allow accurate determination of θ_i, the EWIF sample stage is mounted on a rotation stage and two translation stages. The translation stages are varied so as to ensure that the point of impingement on the surface remains fixed as the rotation stage is turned. Table 1.1 summarizes the properties of some of the most common materials used as IREs.

TABLE 1.1

Material	Transmission Range	Refractive Index (RI)	Density/gcm^{-3}
Fused Silica	170–2300nm	1.46 @ 488nm	2.2
Glass-BK7	330–2500nm	1.52 @ 486nm	2.5
Crown Glass	350–2750nm	1.53 @ 486nm	2.6
Sapphire	300–6000nm	1.78 @ 488nm	4.0
AgCl	420–27000nm	2.00 @ 500nm	5.6

If a disposable surface, such as a microscope slide or coverslip, is added to the arrangement (as in Figure 1.8), it must be optically matched to the IRE so as to minimize the scatter and refraction at the surface/IRE boundary. A further, important consideration in any surface technique is the nature and consistency of the surface used. Since the surface will be slightly different in each experiment, a standard preparation and characterization protocol must be developed, so as to reduce systematic variations between surfaces. Many preparation procedures have been used. However, generally, a surface is cleaned by treatment with organic solvents, followed by hot acid and ultra-pure water. Once treated, the surface "cleanliness" can be confirmed by dynamic contact angle measurements. If sufficiently clean, the surface is used in experiment or further modified by treatment with silanating agents.[27] The use of silanating agents allows the hydrophobicity of the surface to be varied. Since the affinity of a molecule (e.g., a protein) for a surface is dependent on steric, hydrophobic, and electrostatic forces,[1] the careful control of surface characteristics (such as charge and hydrophobicity) can be invaluable in understanding molecule/surface interactions. Furthermore, the techniques of spin- and dip-coating polymers to optical substrates extends the potential number of surfaces open to study.

Fluorescence Detection and Analysis. By virtue of the EWIF sample stage design, the evanescent wave induced fluorescence can be collected either through the sample compartment or through the IRE itself. For simplicity, fluorescence is normally observed perpendicular to the interfacial plane (as indicated in Figure 1.8). This configuration ensures that the reflected beam is excluded from the signal measurement. However, it is noted that as the observation angle approaches grazing angle, the fluorescence detected contains more information about surface associated species compared to bulk phase species (in a fashion analogous to the variation of incident angle). The fluorescence is collected by a condenser lens system (of high numerical aperture) and focused onto the slits of a

monochromator (allowing wavelength selection). Subsequently, the fluorescence is analyzed through the single photon counting (SPC) technique, which provides unrivaled sensitivity in fluorescence detection.[25]

Initially, the fluorescence photons impinge on a photomultiplier tube (PMT). PMTs are high-gain, low-noise light detectors. They can detect single photons over a spectral range of 180 to 900nm. Photons which strike the PMT's photocathode eject an electron by the photoelectric effect. Typically, through a process of repeated, secondary emission the initial electron is amplified to produce about 1,000,000 electrons which are collected by the anode. These electrons produce a millivolt pulse, which can be amplified and then routed to a multichannel analyzer (MCA). The MCA essentially consists of an analog-to-digital converter and a memory containing channels for storing data. The MCA counts the number of pulses in a given time-period and stores the number digitally. If the MCA is operated in multichannel scaling mode and the channel advance is synchronized with the wavelength drive on the monochromator, the resulting histogram of counts in each channel corresponds to the fluorescence spectrum of the fluorophore under investigation. If the monochromator wavelength setting remains constant, the fluorescence variation with time can be monitored through the channel advance. Both these methods of fluorescence analysis are utilized in steady-state TIRFS.

B. Typical Steady-State TIRFS Experiments

Figure 1.9 schematically illustrates a typical molecular adsorption/desorption process. The steps have been vastly simplified for clarity. Figure 1.9A shows a clean solid/liquid interface, free from molecular contamination. After protein solution injection, adsorption begins and protein molecules enter the region illuminated by the evanescent wave (Figure 1.9B). As time progresses, more protein molecules arrive at the surface. This has two effects. First, the fluorophore concentration in the interfacial region increases; and second, conformational changes in the adsorbed layer structure occur, so as to minimize the interfacial free energy of the system (Figure 1.9C). When equilibrium has been reached, the bulk protein solution is removed by a solvent flush. This also removes protein which has been reversibly adsorbed on the time scale of the experiment (Figure 1.9D). If the fluorescence emission of the species under study (e.g., a labeled protein) is monitored with time, then adsorption/desorption kinetics can be elucidated, along with the surface concentration of adsorbed species. A typical TIRF scan (according to Figure 1.9) is depicted in Figure 1.10. After protein injection, a gradual increase in fluorescence intensity is observed due to protein adsorption up to point C. The buffer flush causes the removal of nonadsorbed protein, and this is evidenced by a drop in the fluorescence signal from the evanescent region. The signal levels off at point D, indicating that the residual fluorescence is a result of adsorbed protein.

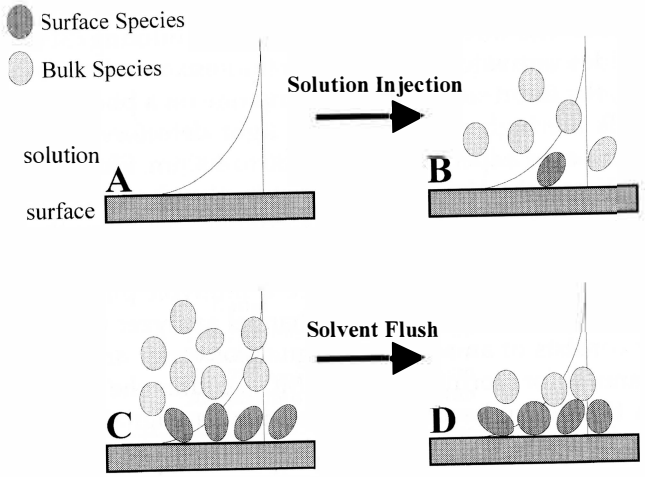

Figure 1.9
Schematic of a typical molecular adsorption process to a solid surface: (A) A solvated solid/liquid interface, (B) Molecules begin to enter the region illuminated by the evanescent wave. Some molecules adhere to the surface displacing solvent molecules, (C) An equilibrium is attained, where both "bulk" and "surface" associated species sit in the region illuminated by the evanescent wave, (D) Solvent flush removes any species from the interfacial region which are not irreversibly adsorbed on the time-scale of the experiment.

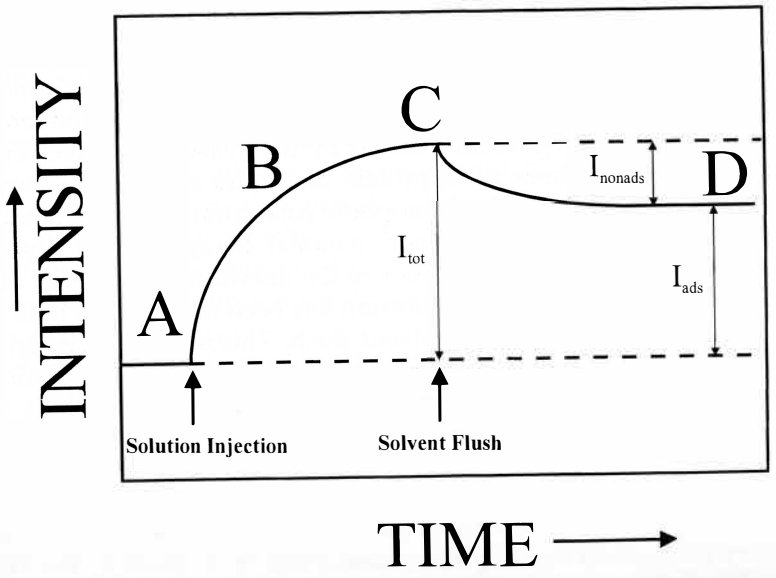

Figure 1.10
Illustration of the idealized TIRF signal corresponding to the molecular adsorption/desorption process indicated in Figure 1.9.

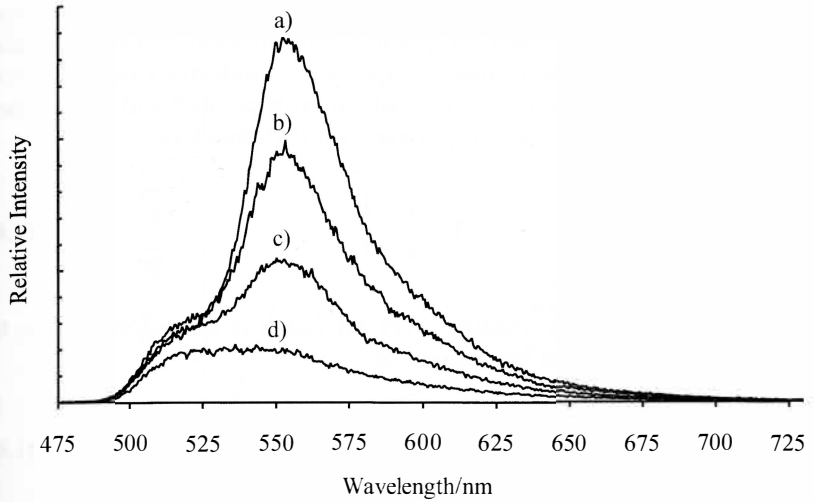

Figure 1.11
Evanescent wave induced fluorescence spectra of poly-4BCMU in 2-MeTHF in contact with a fused silica surface. Spectra were recorded after (a) 2.5, (b) 20, (c) 50, and (d) 195 minutes, following introduction of the solution to an air-dried fused silica surface. (From Rumbles, G., Brown, A. J., Phillips, D., and Bloor, D., *J. Chem. Soc. Faraday Trans.*, 88, 3313, 1992. With permission.)

Furthermore, if fluorescence emission spectra are measured during the experiment, spectral differences between bulk, reversibly adsorbed and irreversibly adsorbed species can be detected. The influence of surfaces on the spectral properties of molecules has been demonstrated unequivocally. For example, Figure 1.11 illustrates the behavior of the conjugated polymer poly-4BCMU in 2-MeTHF in contact with a fused silica surface. The four EWIF spectra shown are taken at times 2.5, 20, 50, and 195 minutes following introduction of the sample to the surface. It is observed that emission shifts to lower energy and becomes more intense with time. The increase in emission is attributed to a reduction in the efficiency of the nonradiative deactivation pathways from the excited state, and the spectral shift is a consequence of the surface inducing a conformational change of the polymer backbone.[19] Other molecules, such as the dyes 1-anilinonaphthalene-8-sulphonate (ANS)[27] and auramine-O,[28] show distinct photophysical changes on interaction with a surface. These variations suggest potential uses as extrinsic markers and labels for biomolecules. For example, ANS has been previously used to quantify BSA (bovine serum albumin) adsorption to modified glass surfaces.

To obtain further information about molecular structure and orientation, TIRFS can be combined with fluorescence polarization measurements. When a collection of fluorophores (e.g., a dye solution) is illuminated with a plane polarized source, only those with a component of their absorption transition dipole moment in the same direction as the polarization vector

will be excited. The probability of absorption is thus proportional to $\cos^2\theta$, where θ is the angle between the plane of polarization and the transition dipole moment. Since, the transition dipoles are randomly oriented, subsequent emission will contain components of both parallel and perpendicularly polarized light. Hence, the polarization P, defined as

$$P = \frac{I_{\parallel} - I_{\perp}}{I_{\parallel} + I_{\perp}} \qquad \textbf{(1.43)}$$

will be less than 1. If averaging over all space is considered, then the intrinsic polarization can be defined as

$$P_o = \frac{3\cos^2\theta - 1}{\cos^2\theta + 3} \qquad \textbf{(1.44)}$$

P_o can take values between 0.5 and –0.33. If the fluorophores are considered to be rigid when excited, $P=P_o$. However, if in the time between absorption and emission, the molecule (and thus the fluorescence transition dipole moment) rotates, photoselectivity is lost and P becomes less than P_o. This means that molecular rotation causes depolarization. Accordingly, the measurement of P is a sensitive probe of molecular motion and reorientations.* If polarization studies of evanescent wave induced fluorescence are made, valuable information about molecular reorientations and conformational changes in the interfacial region can be elucidated. However, unlike conventional electromagnetic radiation where E-fields exist only normal to the direction of propagation, the evanescent wave possesses E-fields in all 3 spatial directions. To account for this difference, Equations 1.31 and 1.32 must be combined with Equation 1.43 in analysis of polarization data. For example, TIRFS has previously been combined with polarization measurements to study the behavior of the conjugated polymer poly-4BCMU in solution near a fused silica surface. Calculated anisotropies indicate that the polymer orders in different ways at the surface, depending on the solvent system used. These ordering processes have important implications in the understanding of how energy is transferred along polymer chains.[19]

C. TIRFS Quantitation

The observed evanescent wave induced fluorescence intensity is given by Equation 1.41. This states that the signal is proportional to the absorption and emission probabilities. Since Δ is also proportional to the concentration of interfacial species, it is theoretically possible to relate fluorescence intensities to surface concentrations. In practice, however, the relationship between I_f and surface concentration is not so direct. The effects of scatter-induced fluorescence and variations in ϕ_f, n_2, and dielectric constant must all be accounted for if surface concentrations can be modeled directly.

* The anisotropy, A, is an extension of the concept of polarization. Anistropy measurements account for the fact that two electric fields rather than one exist perpendicular to the incident axis, and is thus a more useful quantity.[29]

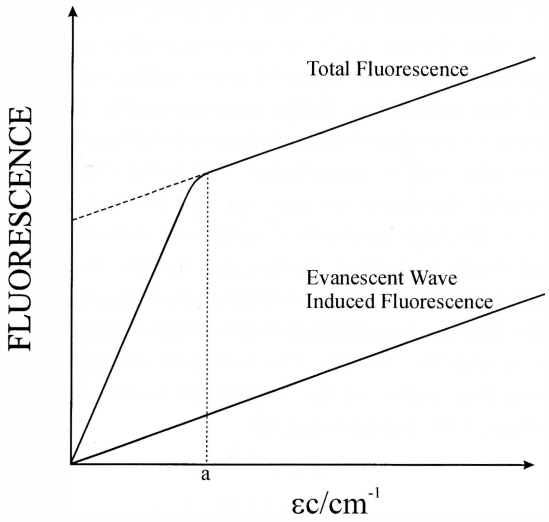

Figure 1.12
Contributions of scatter-induced fluorescence and evanescent wave induced fluorescence to the total fluorescence signal collected. Time "a" represents the point where all scattered excitation light is completely absorbed.

Scatter Induced Fluorescence. Scattering of the incident radiation occurs due to physical imperfections in the optical components of the EWIF sample stage, and also due to incomplete collimation of the incident beam. Since the scattered radiation is propagating in nature, it has the ability to enter medium 2 and excite fluorescence. This fluorescence adds to the evanescently excited signal and may lead to an over estimation of surface concentrations.

The effects of scatter-induced fluorescence can be accounted for by performing a series of experiments in which the bulk concentration of a nonadsorbing species (in medium 2) is sequentially increased.[17] Figure 1.12 illustrates the relationship between bulk solution concentration and fluorescence intensity. The initial part of the graph demonstrates a rapid increase in signal. This is a consequence of increased scatter-induced fluorescence. Since scatter is propagating in nature, a point is reached where all the scattered excitation light is completely absorbed (at time *a*) and re-emitted as fluorescence. Accordingly, any further growth in signal with an increase in bulk concentration is due entirely to evanescent

excitation. If the linear part of the trace is then extrapolated to x=0 and translated along the y-axis until it intersects the origin, the resultant straight line represents the evanescent wave induced fluorescence signal as a function of concentration. If the species under investigation has an appreciable fluorescence quantum efficiency (>10%), the effects of scatter-induced fluorescence will be significant and must therefore be accounted for. Scatter-induced fluorescence can further be minimized by imaging the fluorescence with high numerical aperture collection optics.

Variation of Bulk Solution Refractive Index in the Interfacial Region. The simple interpretation of TIRFS data requires that the refractive index of medium 2 remains constant with distance from the interface. This assumption is not strictly correct. The addition of solute to a solvent will increase the refractive index of the system to some degree. This increase can be approximated by Equation 1.45:

$$n_2 = n_s\left(1+\delta n_2\right) \tag{1.45}$$

Here, n_s is the refractive index of the pure solvent. For protein solutions, δn_2 is defined by

$$\delta n_2 = \left(\frac{c}{n_s}\right)\left(\frac{dn_2}{dc}\right) \tag{1.46}$$

where c is the solution concentration in medium 2, and (dn_2/dc) is the refractive index change of medium 2 per unit increase in solute concentration.[15] Typically, dn_2/dc is of the order of 2.0×10^{-4} ml/mg for protein solutions. Therefore, a solution concentration of 100 mg/ml would cause a 2% increase in the refractive index of medium 2. Although 100 mg/ml represents a high bulk concentration, adsorption to a surface may involve local concentrations of this order. This means that the refractive index in the immediate vicinity of a surface may be appreciably different than the refractive index in bulk solution. Since the characteristics of the evanescent wave are highly dependent on n_{21}, a large change in the interfacial refractive index will affect the measured fluorescence intensities. It is further noted that significantly high surface concentrations may even destroy the TIR regime.

Absorption Effects on the Evanescent Wave. To obtain the concentration distribution of a fluorophore in the vicinity of a surface, the penetration depth of the evanescent wave must be known (Equation 1.34). The working description of the evanescent wave assumes a nonabsorbing medium 2. However, the very basis of the technique requires that energy from the evanescent wave is absorbed. Therefore, the equations in Sections II and III are only approximations. In reality, the absorption of the evanescent wave alters the wavefield conditions in medium 2, which in turn modifies the properties of the evanescent wave.[30] The origin of this modification lies in the refractive index of medium 2.

When a sample is absorbing, the bulk refractive index becomes complex, and may be given by the equation

$$\mathbf{n}_2 = n_2\left(1+ik\right) \tag{1.47}$$

where n_2 (the real part) is the ordinary index of refraction and k is termed the attenuation index. In general, the attenuation index is related to the absorption coefficient, α, by

$$k = \frac{\alpha.\lambda}{4.\pi.n_2} \tag{1.48}$$

Physically, this means that a propagating electromagnetic wave is attenuated as it penetrates an absorbing dielectric. When applied to the phenomenon of TIR, Fresnel's equations become greatly complicated (inspection of Equation 1.4 reveals that $t_\perp$ contains an n_2 term). A rigorous treatment of these new equations demonstrates that the transmitted, evanescent wave is distorted and exhibits a propagating term. The depth of penetration, d_p, is now described by a more detailed function,

$$d_p = \frac{\lambda}{2\pi}\left(\frac{2}{-n_2^2\left(1-k^2\right)+n_1^2\sin^2\theta_i+\left\{\left[n_2^2\left(1-k^2\right)-n_1^2\sin^2\theta\right]^2+4n_2^4k^2\right\}^{1/2}}\right)^{1/2} \tag{1.49}$$

This states that the penetration depth of the transmitted wave is finite, even under the conditions of external reflection. Under TIR conditions the evanescent wave becomes more closely associated with the surface than would be expected if medium 2 were nonabsorbing. Therefore, the more absorbing medium 2 is, the more surface-specific the evanescent wave becomes. The significance and validity of these equations have been thoroughly tested for absorbing samples in many studies.[30] However, it is realized that a general awareness of these effects is sufficient for most experimental analyses.

Variation of Fluorescence Quantum Efficiencies. The majority of TIRFS studies have centered on the quantitation of surface adsorbed species. Various quantitation schemes have been proposed.[16,17] These schemes can be separated into three main areas.

Graphical Quantitation

This involves the use of a nonadsorbing calibration molecule which mimics the properties of the adsorbing species under study. From "bulk" and "surface" fluorescence measurements of both the calibration and adsorbing molecules, the fluorescence signal from adsorbed protein can be estimated. The procedure relies on the assumption that the calibration molecule does not interact in any way with the surface, and also on the fact that any fluorescence quantum efficiency changes are the same for both types of molecule.

Numerical Quantitation

This approach compares the evanescent wave induced fluorescence emanating from nonadsorbed species in the evanescent volume, with fluorescence emanating from adsorbed species. Although commonly used, the analysis of data relies on the assumption that the fluorescence quantum efficiencies of the adsorbed and nonadsorbed species are identical. Furthermore, scatter-induced fluorescence is a significant problem. Hence, fluorescence from nonadsorbed species must be corrected for any scatter contribution prior to comparison.

In Situ *Isotope Quantitation*

This procedure involves the use of a radiolabeled protein which emits γ-radiation with very short pathlengths. Under these conditions, the measured signal is directly proportional to the amount of protein in the evanescent volume. The quantitation process assumes that the radiolabel does not affect protein adsorption isotherms. The use of this technique is limited in elucidating kinetic and conformational information about molecular adsorption.

In conclusion, it is observed that the complete quantitation of steady-state TIRFS data is beset by significant problems. All internal calibration methods assume that fluorescence quantum efficiency changes are negligible upon adsorption. This assumption is unacceptable, and therefore steady-state TIRFS is only semi-quantitative. To make the technique fully quantitative, the fluorescence quantum efficiencies of bulk phase and surface-associated species must be determined. This can be achieved by extending the technique of TIRFS into the time domain.

V. TIME-RESOLVED TIRF SPECTROSCOPY

A. Theoretical Aspects

The fluorescence quantum yield (or more correctly, the fluorescence quantum efficiency) described in Equation 1.40 defines the fraction of

excited state species that become de-excited by fluorescence. If the only means of depopulating the excited state is through fluorescence (radiative deactivation), then the process has a relaxation time given by the reciprocal of k_r. The relaxation time is commonly referred to as the *radiative* or *natural* lifetime, τ_r. Normally, nonradiative processes compete with fluorescence, thus reducing the lifetime of the excited state. The experimentally determined fluorescence lifetime, τ_f, can thus be defined by

$$\tau_f = \frac{1}{k_r + k_{nr}} \qquad \textbf{(1.50)}$$

Combination of Equations 1.50 and 1.40 yields an alternative expression for the fluorescence quantum efficiency,

$$\phi_f = \frac{\tau_f}{\tau_r} \qquad \textbf{(1.51)}$$

Since the radiative lifetime of a fluorophore can be calculated through use of the Strickler-Berg relationship,[31] variations in the fluorescence quantum efficiency of a fluorophore can be detected through changes in the magnitude of the fluorescence lifetime. If Equation 1.51 is recombined with Equation 1.42 a complete description of evanescent wave induced fluorescence can be developed, i.e.,

$$I_f \propto k_r \int_0^\infty \tau_f(x).c(x).I_0 \exp(-x/\Lambda)dx \qquad \textbf{(1.52)}$$

Since the radiative rate constant should be essentially invariant, any changes in the fluorescence lifetime can be used to directly calculate interfacial concentrations from evanescent wave induced fluorescence measurements. In practice, the measurement of fluorescence quantum efficiency changes is achieved through combination of TIRFS with the technique of time-correlated single-photon counting (TCSPC).[25] The technique relies on the concept that the probability distribution for emission of a single photon after excitation, yields the intensity versus time distribution for all photons emitted. Experimentally, this is achieved by sampling single photon emission for a large number of excitation events. The basic principles of TCSPC are best summarized through use of a simple block diagram, Figure 1.13.

A light source emits an optical pulse which is used to excite fluorescence from the sample under study. At a time exactly correlated with the generation of this pulse, an electrical pulse is generated by a trigger. The electrical pulse is routed, via a discriminator, to the "start" input of the time-to-amplitude converter (TAC). This initiates the charging of an in-

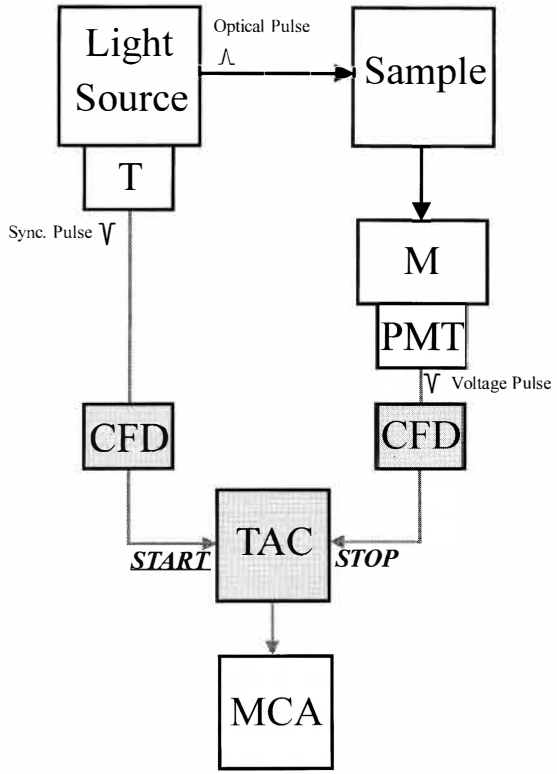

Figure 1.13
Schematic arrangement for time-correlated single-photon counting. T- Trigger, M - Monochromator, PMT - Photomultiplier Tube, CFD - Constant Fraction Discriminator, TAC - Time-to-Amplitude Converter, MCA - Multichannel Analyzer. The CFD is used to reject pulses outside a certain amplitude range and so improve the timing characteristics of the technique.

produces a voltage pulse that is routed to the "stop" input of the TAC. This stops the charging ramp in the TAC and yields an output pulse with an amplitude proportional to the charge on the capacitor (and thus proportional to the time delay between start and stop pulses). Subsequently, the output pulse is fed into a multichannel pulse-height analyzer, which stores the pulses by voltage. Excitation is repeated until a histogram of intensity versus time is built up.

If the optical pulse was infinitely narrow and the response of the detection system infinitely fast, the observed decay would represent the true fluorescence decay. However, in reality the optical pulse has a finite width, and the response of the detection system is not instantaneous. Consequently, the response of the system must be deconvoluted from the observed decay to yield the true decay profile (the response of the system is determined by replacing the sample with a scattering solution, and repeating the TCSPC experiment). The decaytime can then be obtained

by calculating the time required for the intensity of the true decay function to decrease by a factor of 1/e. Details of the deconvolution procedures are widely documented.[25,32,33]

B. Instrumentation

The experimental set-up for the time-resolved experiment is similar to the steady-state methodology. Consequently, only brief details of the full system are discussed.

The Light Source. Today, the most common light source used in a TCSPC experiment is a pulsed laser system. Typically, the 2nd or 3rd harmonic (532 or 355 nm) of a mode-locked Nd:YAG laser is used to synchronously pump a cavity-dumped dye laser. This results in the production of 10 ps pulses at high repetition rates. Significantly, the use of different dyes permits a wide range of excitation wavelengths (200 to 1300nm). The choice of laser system is dependent on both the absorption characteristics of the sample and the time-resolution required. Most current TCSPC systems can resolve fluorescence lifetimes below 20 ps without much trouble.

The EWIF Sample Stage. The EWIF sample stage is identical to that used described in Section IV.A.

Fluorescence Detection and Analysis. Evanescent wave induced fluorescence is collected by a condenser lens (high numerical aperture) and focused onto the slits of a monochromator. Subsequently, the fluorescence is detected by a photomultiplier tube and processed as described in Section V.A. A sync pulse from the cavity-dumper driver provides the "stop" signal for the TAC.

TABLE 1.2

Sample	$I_{ewif} : I_{bulk}$
Species A	0.05
Species B	1

C. Applications of Time-Resolved TIRFS

As stated, the initial application of time-resolved TIRF measurements is in the quantitation of fluorescence quantum efficiency changes. The combination of both the steady-state and time-resolved data allows evanescent wave induced fluorescence intensities to be directly related to surface concentrations. For example, Table 1.2 illustrates the ratio of evanescent wave induced fluorescence intensity to bulk fluorescence intensity (I_{ewif}:I_{bulk}) for two species. Sample A is a nonadsorbing calibration molecule, and sample B is the species under investigation. It can be seen that for sample B the fluorescence intensity originating from the evanescent region is far greater than predicted from its bulk concentration. Alone,

this observation implies that either, (a) the interfacial concentration of species B is significantly higher than A (i.e., adsorption has occurred), or (b) the fluorescence quantum efficiency of species B is enhanced when in the vicinity of the surface. To establish the real reason for the observed increase in fluorescence intensity, time-resolved TIRF measurements are performed. If the fluorescence lifetime of species B in the vicinity of the surface is the same as in bulk solution, it can be concluded that adsorption has occurred. However, if the fluorescence lifetime of species B in the interfacial region is greater than the bulk lifetime, then the fluorescence quantum efficiency of B has increased, and the situation becomes more complicated.

Time-resolved TIRF spectroscopy has been used to investigate the photophysical properties of the dye auramine-O at a solid/solution interface.[28] In free solution, the fluorescence decaytime of the molecule is very short (<10 ps). However, interaction of the dye with a glass surface causes a significant enhancement of the fluorescence quantum efficiency, through restriction of intramolecular rotations. This is evidenced by both an increase in fluorescence intensity at the surface and a lengthening of the excited state decaytime (<500 ps). Figure 1.14 illustrates examples of both bulk and evanescent wave induced fluorescence decays. It can be seen that the "surface" decay kinetics are significantly longer than the "bulk" decay kinetics. Further inspection of the evanescent wave induced fluorescence decay highlights the most significant problem in assessing quantum yield changes. Equation 1.52 requires an exact knowledge of $\tau_f(x)$, i.e., the model assumes that the evanescent wave induced fluorescence decay can be described by a single exponential relaxation time. However, the decay shown in Figure 1.14b is complex, and a single exponential lifetime does not adequately describe the profile. In fact, the decay can only be successfully paramaterized by a sum of three exponentials model. This complexity is typical of most EWIF decays. To overcome this problem, an average lifetime is constructed from the components of the decay, thus allowing an estimation of $\phi_f(x)$.

Although it is apparent that surfaces can induce changes in the photophysics of many molecules, the nature of these changes is not altogether understood. Adsorption of a molecule to a surface will result in a diversity of interactions between the surface and other molecules. Even "well defined" surfaces will accommodate a variety of "interfacial environments." If this picture is correct, then it would be expected that the sum of interactions which add to the radiative and nonradiative deactivation pathways will yield a distribution of fluorescence lifetimes, as opposed to a single lifetime. This supports the heterogeneity observed in most "surface" decays.[26,34,35]

Lifetime distribution analysis (LDA) provides a significant improvement on existing fitting routines.[32,36] The general procedure allows differentiation of decays made up of two or three discrete components from systems possessing a continuous distribution of lifetimes (e.g., interfacial

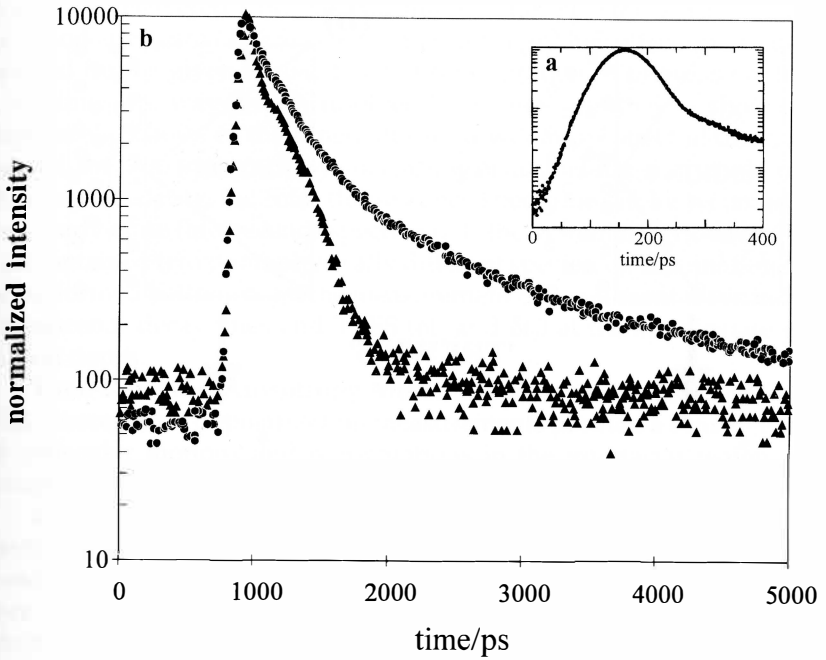

Figure 1.14
(a) Fluorescence decay profile of auramine-O in water (10^{-5} M), (b) Evanescent wave induced fluorescence decay profile of auramine-O at a glass/water interface. Instrument response function ~ 80 ps FWHM, λ_{ex} = 430 nm and Λ = 80 nm. (From de Mello, A. J., Crystall, B., and Rumbles, G., *J. Colloid Interface Sci.*, 169, 161, 1995. With permission.)

systems). The application of LDA to time-resolved TIRFS measurements has recently been reported.[28] It is noted that a more complete analysis of "surface" decay profiles is available through the use of LDA techniques. However, conventional fitting routines provide a good working model and can be successfully used to obtain information about fluorescence quantum efficiency changes. In particular, the use of global analysis procedures allows simultaneous analysis of multiple data sets. Although the analysis procedure is still model dependent, the application of a given model over a multidimensional data surface is as statistically rigorous a test of a particular model as can be performed.[32]

In addition to quantifying steady-state TIRFS measurements, time-resolved studies provide invaluable information about the environment, conformation, and orientation of interfacial species.

Decay times. In many instances, the number of measured lifetimes is a reflection of the number of noninteracting species contributing to the decay. Consequently, in multicomponent systems, the shape of the decay profile is a sensitive probe of the identity of interfacial species. Figure 1.15 represents an idealized two-component system. Region 1 is the IRE, region 2 is a layer of fluorophores with a fluorescence decaytime τ_1, and region

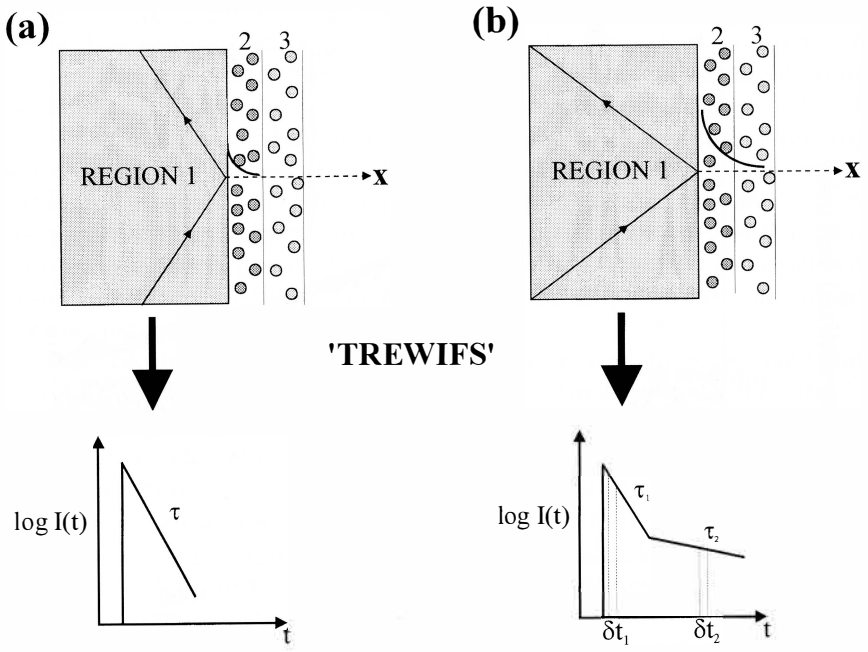

Figure 1.15
Schematic demonstration of the ability of TREWIFS to discriminate between interfacial species. (a) TIR geometry generates an evanescent wave closely associated with the surface. The fluorescence decay is only characteristic of species in region 2 (τ_1). (b) TIR geometry generates an evanescent wave less closely associated with the surface. The fluorescence decay now contains information about species in both regions 2 and 3 (τ_1 and τ_2).

3 a secondary layer of fluorophores with a fluorescence decaytime τ_2. In Figure 1.15a the incident angle is such that the penetration depth of the evanescent wave is shallow. Accordingly, only fluorophores in region 1 are excited by the evanescent wave, and the observed decay profile is monoexponential. Figure 1.15b represents the situation where the penetration depth of the evanescent wave has been increased (through a reduction in the angle of incidence). Now, both sets of fluorophores are excited by the evanescent wave and the observed decay profile becomes biexponentional. The power of the time-resolved measurement (compared to steady-state measurements) lies in its ability to distinguish between species with similar spectral characteristics. For example, if the species in region 2 were quenched forms of the species in region 3, the spectral characteristics of both 1.15a and 1.15b could be identical. It is only the kinetic data that discriminate. Many time-resolved TIRFS on these lines have been performed to good effect.[28,32]

Time-Resolved Emission Spectra. Time-resolved emission spectroscopy can yield important information about photophysical equilibria that

cannot be recovered from normal fluorescence spectra. A time-resolved emission spectrum (TRES) is generated through the collection of photons emitted from a given time-gate (δt) after excitation. If photons emitted at long times are wavelength resolved from those emitted at short times, then careful choice of the time-gates used will allow spectral discrimination of the two species.[25] By increasing δt to include the whole of the fluorescence decay, the total fluorescence spectrum can be recorded (i.e., the steady-state fluorescence spectrum). If the system described in Figure 1.15 contained two photophysically different species, discrimination could be performed both through the measurement of evanescent wave induced fluorescence decaytimes and TRES (δt_1 and δt_2) at the appropriate penetration depth.

Time-Resolved Anisotropy Measurements. As discussed in Section IV.B, fluorescence depolarization measurements provide a sensitive probe of molecular motions and reorientations in the interfacial region when combined with TIRFS.

If a sample is excited by an optical pulse, the intensity of fluorescence emitted parallel and perpendicular to the direction of excitation can be measured as a function of time (using TCSPC). There is an initial difference in intensity (due to photoselection), which typically decays after a few nanoseconds as the molecule rotates. If A_o is defined as the initial anisotropy, the anisotropy at time t (A(t)) can be related to the rotational correlation time, τ_R, by

$$A(t) = A_o \exp(-t/\tau_R) \qquad \textbf{(1.53)}$$

If there is more than one molecular motion, then the decay is analyzed as a sum-of-exponentials to elucidate the contribution of each movement. Comparison of bulk phase behavior with surface behavior can be extremely revealing. If a species interacts with a surface, it is expected that certain rotational motions will be hindered or perturbed. These changes should be evidenced in the form of the anisotropy decay.[29]

D. Current Limitations of Time-Resolved TIRFS

The only significant questions surrounding the technique lie in (1) the assumption that the radiative rate constant is invariant, and (2) the interpretation of the interfacial decay profiles.

Equation 1.52 separates the radiative rate constant from the integrated term, i.e., it is assumed that k_r is the same in the vicinity of the interface as it is in bulk solution. Previously, it has been shown that k_r does have a dependence on the refractive index of the local environment.[37] This dependence can be mathematically represented by

$$k_r \propto n^2 \int \left[\frac{\varepsilon(\upsilon)}{\upsilon} \right] d\upsilon \qquad \textbf{(1.54)}$$

Here, the integrated term describes the area under the absorption spectrum of the emitting fluorophore (ε is the molar extinction coefficient, and υ is frequency). If there are local fluctuations in the refractive index of medium 2 (e.g., through molecular adsorption to the surface), then k_r is likely to vary. However, these variations should be relatively small, and the assumption that k_r is invariant will hold for most systems.

The complexity introduced into EWIF decays, as a result of the heterogeneity of the interfacial environment, hinders complete quantitation of the fluorescence quantum efficiency changes. The nature of surface-molecule interactions appears to be significant in determining the shape of the decay profile, and it appears that a true understanding of "interfacial" kinetics lies in the use of LDA techniques to describe the EWIF decays.

VI. CONCLUSIONS AND FUTURE TRENDS

The suitability of a particular technique to the study of molecular adsorption was judged in Section I.A on how well it fulfilled a seven-point plan. Subsequently, it has been shown that the association of steady-state and time-resolved TIRFS can accomplish many of the requirements listed. Surface concentrations can be calculated through the combination of evanescent wave induced fluorescence intensity measurements and decaytime data. Conformational changes can be inferred from variations in spectral and kinetic data. Modification of λ_{vac}, θ_i, and n_{21} allows sensitive control of surface specificity, thus ensuring differentiation between bulk and surface-associated species, and a variety of modified surfaces are available to study (although the substrate must be transparent). One significant advantage of TIRFS over other analysis techniques is its nondestructive nature. Many highly sensitive surface analysis techniques exist, but most either require high vacuum conditions or destroy the sample. Finally, the technique permits real-time monitoring of adsorption/desorption processes. This is of particular significance in the study of the thrombogenic response of the blood to biomaterial surfaces.

Although TIRFS offers a number of advantages over existing surface analysis techniques, there are obvious limitations. Any optical technique is restricted by the light source available. As noted, a wide range of wavelengths is available to the experimenter, however, pumped dye laser systems are expensive, and the UV spectral region is often difficult to access. If a large biomolecule is labeled with a smaller fluorophore, it is assumed that the label does not affect the physical characteristics of the parent molecule. This is normally valid, as long as the parent molecule is significantly larger than the label. However, some physiochemical changes may occur and affect adsorption.

Recent developments in the field of mode-locked/cavity-dumped lasers have enabled the production of femtosecond optical pulses. High repetition rate, high intensity sources of narrow spectral line width have ensured that efficient TCSPC can be performed on species with decaytimes below 10 ps. When combined with total internal reflection geometry, important chemical processes (such as electron-transfer, proton-transfer, molecular reorientations, and energy transfer) occurring in interfacial regions can be monitored. In addition, modern surface preparation and characterization techniques will undoubtedly improve the reproducibility of interfacial fluorescence intensities and decaytimes. The continued application of LDA fitting routines should also provide "physical significance" to the evanescent wave induced fluorescence decay forms. The interfacial region is one of unquestionable heterogeneity. Molecule–molecule and molecule–surface interactions create an extremely complex environment. As surface concentrations are reduced, the decay kinetics should, in principle, become simpler. Although, this progression is observed in experiment, the reduction in "surface" concentration causes a corresponding decrease in the fluorescence signal, and thus the observed "simplicity" is limited by the detection system.

In conclusion, TIRFS does offer a sensitive and dynamic method for investigating interfacial phenomena. Its advantages outweigh its current limitations, and continued research efforts will only improve this situation. The power of the technique lies in its ability to probe molecular phenomena in the interfacial environment, rather than providing precise information about the amount of adsorbed species. Nevertheless, quantification of adsorbed species is of paramount importance to the biomaterialist, and hence the technique still remains in a formative stage as an analytical tool. The primary hurdle to surmount here will be a complete description of fluorescence kinetics in the interfacial region.

The study of the solid/liquid interface has many significant applications in the fields of molecular assembly, biosensors, molecular electronics, and biomaterial design. Consequently, the future of TIRFS as a surface analysis technique looks a healthy one.

ACKNOWLEDGMENTS

The concepts and theories discussed in this chapter are drawn from a wealth of research performed over the last 25 years. Special recognition must be extended to G. Rumbles, V. Hlady, N.J. Harrick, D. Phillips, and W.M. Reichert, whose work has been particularly influential in the writing of this chapter.

REFERENCES

1. Andrade, J. D., Ed., *Surface and Interfacial Aspects of Biomedical Polymers*, Vol. 1 and Vol. 2, Plenum Press, New York, 1985.
2. Vroman, L. and Leonard, E. F., Eds., Behaviour of Blood and its Components at Interfaces, *Ann. N. Y. Acad. Sci.*, 283, 1977.
3. Brash, J. L., Mechanism of Adsorption of Proteins to Solid Surfaces, in *Biocompatible Polymers*, Szycher, M., Ed., Technomic, Lancaster, 35, 1983.
4. MacRitchie, F., *Adv. Prot. Chem.*, 32, 283, 1978.
5. Poste, G. and Moss, C., *Prog. Surf. Sci.*, 2, 139, 1972.
6. Ho, C-H., Hlady, V., Nyquist, G., Andrade, J. D., and Caldwell, K. D., *J. Biomed. Mat. Sci.*, 25, 423, 1991.
7. Walton, A. G. and Maenpa, F. C., *J. Colloid Interface Sci.*, 72, 265, 1979.
8. Sperline, R. P., Muradlidharan, S., and Feiser, H., *Langmuir*, 3, 198, 1987.
9. Absolom, D. R., Van Oss, C. J., Zingg, W., and Neumann, A. W., *Biochim. Biophys. Acta*, 670, 74, 1981.
10. Cotton, T. M., Surface Enhanced Raman Spectroscopy of Biological Macromolecules, in *Surface and Interfacial Aspects of Biomedical Polymers*, 2, Plenum Press, New York, 161, 1985.
11. Liedberg, B., Nylander, C., and Lundstrom, I., *Sensors and Actuators*, 4, 299, 1983.
12. Van de Scheer, A., Feijen, J., Elhorst, J. K., Dagneaux, P. G. K., and Smolders, C. A., *J. Colloid Interface Sci.*, 66, 136, 1978.
13. Harrick, N. J., *Internal Reflection Spectroscopy*, Interscience-Wiley, New York, 1967.
14. Hirschfield, T., *Can. Spectroscopy*, 10, 128, 1965.
15. Reichert, W. M., *CRC Rev. Biocompatibility*, 5, 173, 1989.
16. Hlady, V., Van Wagenen, R. A., and Andrade, J. D., Total Internal Reflection Intrinsic Fluorescence (TIRIF) Spectroscopy Applied to Protein Adsorption, in *Surface and Interfacial Aspects of Biomedical Polymers*, Plenum Press, New York, 2, 81, 1985.
17. Hlady, V., Reinecke, D. R., and Andrade, J. D., *J. Colloid Interface Sci.*, 111, 555, 1986.
18. Toriumi, M. and Masuhara, H., *Spectrochimica Acta Rev.*, 14, 353, 1991.
19. Rumbles, G., Bloor, D., Brown, A. J., de Mello, A. J., Crystall, B., Phillips, D., and Smith, T. A., Time-Resolved Evanescent Wave Induced Fluorescence Studies of Polymer-Surface Interactions, in *Microchemistry: Spectroscopy & Chemistry in Small Domains*, Masuhara, H., Ed., Elsevier Science, Netherlands, 269, 1994.
20. Born, M. and Wolf, E., *Principles of Optics*, Pergamon Press, Oxford, 1970.
21. Newton, I., *Opticks*, Dover Publications, New York, 1952.
22. Maxwell, J. C., *A Treatise on Electricity and Magnetism* (Vols. 1 and 2), Oxford, 1873.
23. Goos, F. and Hänchen, H., *Ann. Physik*, 6, 333, 1947.
24. Birks, J. B., *Photophysics of Aromatic Molecules*, Wiley-Interscience, London, 1970.
25. Phillips, D. and O'Connor, D. V., *Time-Correlated Single-Photon Counting*, Academic Press, London, 1984.
26. Rumbles, G., Brown, A. J., and Phillips, D., *J. Chem. Soc. Faraday Trans.*, 87, 825, 1991.
27. Hlady, V., Gölander, C., and Andrade, J. D., *Colloids Surfs.*, 25, 185, 1987.
28. de Mello, A. J., Crystall, B., and Rumbles, G., *J. Colloid Interface Sci.*, 169, 161, 1995.
29. Steiner, R. F., Fluorescence Anisotropy: Theory and Applications, in *Topics in Fluorescence Spectroscopy*, Volume 2: Principles, Lakowicz, J. R., Ed., Plenum Press, New York, 1, 1991.
30. Toriumi, M., Yanagimachi, M., and Masuhara, H., *Appl. Opt.*, 31, 6376, 1992.
31. Strickler, S. J. and Berg, R. A., *J. Chem. Phys.*, 37, 814, 1962.
32. de Mello, A. J., PhD Thesis, University of London, 1995.
33. Birch, D. J. S. and Imhof, R. E., Time-Domain Fluorescence Spectroscopy using Time Correlated Single Photon Counting, in *Topics in Fluorescence Spectroscopy*, Volume 1: Techniques, Lakowicz, J. R., Ed., Plenum Press, New York, 1, 1991.

34. Bell, M. A., Crystall, B., Rumbles, G., Porter, G., and Klug, D. R., *Chem. Phys. Lett.*, 221, 15, 1994.
35. Liu, Y. S., deMayo, P., and Ware, W. R., *J. Phys. Chem.*, 97, (5980, 5987, 5995), 1993.
36. James, D. R. and Ware, W. R., *Chem. Phys. Lett.*, 126, 7, 1986.
37. Hirayama, S. and Phillips, D., *J. Photochem.*, 12, 139, 1980.